# Simulations and Measurements of In-Mold Melt Flow During the Injection Molding of Polystyrene

**Thomas J. Bress, David R. Dowling**
*Department of Mechanical Engineering, University of Michigan, Ann Arbor, Michigan*

**Simulations are often used to model polymer flow during injection molding to design molds and select processing parameters. It is difficult to determine the accuracy of these simulations due to a lack of experimentally measured in-mold velocimetry and melt-front progression data. This article compares the results from commercial mold-filling simulation software to experimental data obtained via particle image velocimetry (PIV) in a special optical-access mold with a rectangular cavity. Moldflow was used to simulate the mold filling by a polystyrene melt in the experimental configuration, and these simulated results are compared to the appropriately averaged time-varying velocity field measurements. Simulated results for melt-front progression are also compared with experimentally observed flow fronts. The ratio of the experimentally measured average velocity magnitudes to the simulation magnitudes was found on average to be 0.99 with a standard deviation of 0.25, and the difference in velocity orientations was found to be 0.9° with a standard deviation of 3.2°. The corner area opposite the gate was most problematic for the simulation. The region behind the front also had a relatively high simulation error, though not as severe as that in the corner. POLYM. ENG. SCI., 53:770–779, 2013. © 2012 Society of Plastics Engineers**

## INTRODUCTION

Injection molding is one of the most common and most important methods of processing polymers. Mold filling is a critical step in the injection molding process, influencing dimensional stability, mechanical properties, residual stresses, warpage, and part-to-part consistency [1]. Thus, mold-design work often involves simulations of the unsteady three-dimensional non-Newtonian polymer melt flow that occurs during mold filling, and molding engineers commonly use simulations to design molds and select processing parameters. Computational polymer fluid dynamics is an active area of research and commercial codes are available for predicting melt flow during the mold filling stage of the injection molding process [2]. Here simulation accuracy can help reduce mold development times and ensure appropriate final part properties. In-mold pressure measurements have been reported and have been used for process control and comparison with simulations [3]. However, quantitative experimental information from which to assess the accuracy of the mold-filling velocity field simulations is scarce. This article presents a unique quantitative study of simulated and measured polymer-melt velocity fields and melt-front motion during injection molding of polystyrene within a nominally rectangular mold cavity.

The work reported here extends beyond flow visualization into the realm of velocimetry. Injection molding flow visualization has a long history, and such results have often been used to benchmark computer simulation results. Early injection-molding flow-visualization work was largely qualitative [4], and visualization studies were typically performed to examine polymer melt flow fronts [5, 6]. These studies were used to validate theoretical and computational models of injection molding flow [7, 8] but did not provide full-field velocity data. More recent (and more quantitative) melt flow visualization studies have been done to study shrinkage [9], melt front propagation [10], the generation of wave-like flow marks [11], and the filling of microscale V-grooves [12]. These more recent studies, however, do not provide the polymer-melt velocity field data that is possible with particle image velocimetry (PIV), a common Newtonian-fluid velocimetry technique [13].

Non-Newtonian velocimetry studies that provide full-field velocity data have been done and these studies are quantitative. However, such studies typically do not involve unsteady flows or molten plastics that solidify, tending to focus instead on steady flow of non-Newtonian fluids in idealized geometries [14].

The scarcity of in-mold flow data is due to the fact that injection-molding flow nearly always takes place in a closed metal mold at elevated temperatures and pressures. The polymer melt itself is generated from solid plastic pellets within the injection molding machine and this leads to further difficulties related to seeding the flow for experimental measurement of velocities. In typical PIV studies, particles such as silvered glass spheres are mixed with the fluid that is to be studied. But in injection mold-

*Correspondence to*: Thomas Bress; e-mail: tbress@exponent.com
Contract grant sponsor: Colonial Engineering Inc.
DOI 10.1002/pen.23321
Published online in Wiley Online Library (wileyonlinelibrary.com).

ing, these particles need to be added to the hopper of the injection molding machine with the solid plastic pellets. Standard PIV particles cannot withstand the high-shear environment inside the barrel of the injection molding machine. Also, the seeding density of the particles can be easily controlled but not the seeding distribution. The injection molding machine itself mixes the particles into the molten plastic as the pellets travel through the barrel of the injection molding machine. In addition to these access and seeding difficulties, melt flow in an injection molding machine is challenging to measure because it is unsteady, non-Newtonian, non-isothermal, and includes solidification.

Recently, real time velocity vector field data for polystyrene flowing into a corner-gated rectangular mold have been reported [15], and the present study follows from this prior effort. An optical access mold was constructed that allowed passage of a laser sheet through the midplane of the mold [16]. STYRON 615APR was seeded with 0.02% by weight aluminum flakes and digital particle velocimetry (DPIV) [17] was used to extract the time-varying velocity field at the midplane of the mold. Flow front geometry as a function of time was also extracted from the image data. The experimental details and results are given in [15].

The results from that study can be used to benchmark melt-flow simulations. For the current study, Moldflow Plastics Insight was chosen for this purpose since it is widely used in industry. Based on mold geometry, plastic material properties, and injection conditions, Moldflow predicts time-varying average velocity fields and melt front locations. In the present work Moldflow was used to simulate the melt flow observed in [15], and the experimental data and simulation results are compared to assess the accuracy of the simulations.

### *Simulating Polymer Melt Flow With the Hele–Shaw Approximation*

The Hele–Shaw model is typically used to model polymer melt flow in the mold cavity [2]. The Hele–Shaw model equation is given by [18]:

$$\nabla \cdot (S \nabla p) = 0 \tag{1}$$

where $S$ is the flow conductance and is given by:

$$S(x,y) = \int_0^B \frac{z^2 dz}{\eta(x,y,z)} \tag{2}$$

and $\eta$ is the local viscosity and $B$ is the cavity half-thickness. The gap-wise average velocities are given by

$$u_{\text{mean}} = \frac{S}{B} \nabla p \tag{3}$$

### *Ramifications of the Hele–Shaw Model on the Simulation of Polymer Melt Flow*

The Hele–Shaw model has limitations that can be expected to cause deviations between simulation results and experimental data. One limitation is that the Hele–Shaw approximation does not satisfy the full continuity equation $\nabla \cdot \vec{u} = 0$. It instead satisfies an integrated continuity equation, a weaker requirement. This can be seen by combining *Eqs. 1* and *3*:

$$\nabla \cdot (B u_{\text{mean}}) = 0 \tag{4}$$

Another limitation is that no-slip or prescribed-slip boundary condition cannot be imposed when using the Hele–Shaw model. Dirichlet boundary conditions are typically imposed for *Eq. 1*. At the melt front the pressure is zero, and at the gate the injection pressure is specified. At the solid boundaries of the mold cavity Neumann boundary conditions are imposed with $\partial p / \partial n = 0$. Because the velocity is proportional to the pressure gradient, *Eq. 3* shows that this is equivalent to imposing a no-penetration boundary condition at the walls. These boundary conditions completely specify the solution of *Eq. 1*, so a no-slip or prescribed-slip boundary condition cannot be imposed when using the Hele–Shaw model. *Equation 3* shows that the velocity is parallel to the pressure gradient. There will always be a pressure gradient parallel to the wetted surface of the mold [2], so there will always be a nonzero tangential velocity at the walls of the mold when using the Hele–Shaw model. The magnitude of this tangential velocity cannot be set to zero or otherwise specified as a boundary condition when using the Hele–Shaw model.

Another limitation is that the Hele–Shaw model has difficulty modeling flow fronts accurately near cavity walls. Mold-filling simulation software such as Moldflow uses the calculated pressure distribution to generate average velocities, and then uses these velocities to move the polymer in the cavity. Along the cavity walls the imposed boundary condition is $\partial p / \partial n = 0$. This means that isobars will always be perpendicular to the cavity walls at the point of intersection with the wall. Because the flow front is also an isobar with $P$ equal to zero the flow fronts will tend to be perpendicular to the cavity walls.

Finally, the Hele–Shaw model assumes negligible polymer velocity in the thickness direction. This is a good approximation for polymer melt flows in most areas of the mold cavity, but it does not hold true near the flow front due to the fountain flow effect [19]. Molten polymer in a thin-cavity mold does travel in a two-dimensional fashion for the most part. Melt velocities in the mold cavity do not have a significant component perpendicular to the midplane of the mold except in the region near the melt front. As molten plastic approaches the melt front it develops a significant velocity component perpendicular to the midplane, causing the melt to turn towards the

TABLE 1. Cross-WLF parameters for STYRON615 APR with 0.02% by weight loading of aluminum flakes as measured by Moldflow Plastics Labs.

| | |
|---|---|
| $n$ | 0.372 |
| $\tau$ | 21765.5 Pa |
| D1 | 4.325e10 Pa $s^{-1}$ |
| D2 | 373.15 K |
| D3 | 0 K/Pa |
| A1 | 25.245 |
| A2 | 51.600 K |

cavity walls. Viewed from the edge of the mold and from a frame of reference attached to the front, the flow looks fountain. Fountain flow takes place perpendicular to the midplane of the cavity and thus cannot be quantified using the Hele–Shaw model.

## EXPERIMENTAL RESULTS

Bress and Dowling [15] used digital particle image velocimetry (DPIV) to measure midplane velocity vector fields throughout the mold filling process. An optical access mold was built to allow passage of a pulsed laser sheet through the midplane of a corner-gated nominally rectangular cavity 109.5 mm × 66.7 mm × 6.3 mm (4 5/16″ by 2 5/8″ by 0.25″). The molten plastic was STYRON 615APR loaded with 0.02% by weight aluminum flakes. Polystyrene was chosen for this study because it was transparent, easy to mold, and commonly used in industry. The mold also allowed visualization of the flow through the 109.5 mm × 66.7 mm face of the cavity [16]. A CCD camera with a resolution of 600 × 480 pixels and a frame rate of 30 Hz was used to make digital movies of the mold filling process. The camera was also used to drive a pulsed laser, generating a single 6–7 ns pulse of laser light in each movie frame to freeze the motion of the polymer melt. The laser light was scattered from the aluminum flakes at the midplane of the melt flow and standard DPIV techniques were used to calculate the melt velocity fields from the digital images. Flow fronts were also manually extracted from the digital movie images.

The viscosity curves of the polymer and particle mixture were measured by Moldflow Plastics Labs using an injection molding capillary rheometer. Cross-WLF model parameters were extracted from this data by Moldflow Plastics Labs and are presented in Table 1.

Midplane velocity fields for an injection rate of 34.5 $cm^3\ s^{-1}$ and a melt temperature of 245°C are shown in Figs. 1 and 2. Here the largest two dimensions of the nominally rectangular mold cavity are displayed vertically and horizontally. The gate is in the lower left corner of the mold. The vector fields shown correspond to values of $t^*$ equal to 0.3, 0.5, 0.7, and 0.9 where $t^*$ is time normalized by the mold filling time. Reliable PIV measurements could not be made within 4 cm of the gate because of the strong radial flow in that region and the finite temporal resolution of the digital camera used for particle-image acquisition. In a strong radial flow PIV particles separate from their neighbors leading to failure of the cross-correlation process [15]. Thus, the vector-free zone nearest the gate in each frame of Figs. 2 and 3 is intentional.

### *Estimating the Mean Cavity Velocity From the PIV Data*

Moldflow uses the Hele–Shaw approximation to calculate a mean velocity averaged through the cavity thickness. The PIV data measures the maximum velocity through the cavity thickness, the velocity at the midplane of the mold. To compare the two data sets the maximum velocities at the midplane of the cavity must be used to estimate the average velocities through the cavity thickness at the same points.

This can be done using the known polymer-melt injection rate and by making the assumption that the average velocity magnitude $u_{mean}$ at a given point is proportional

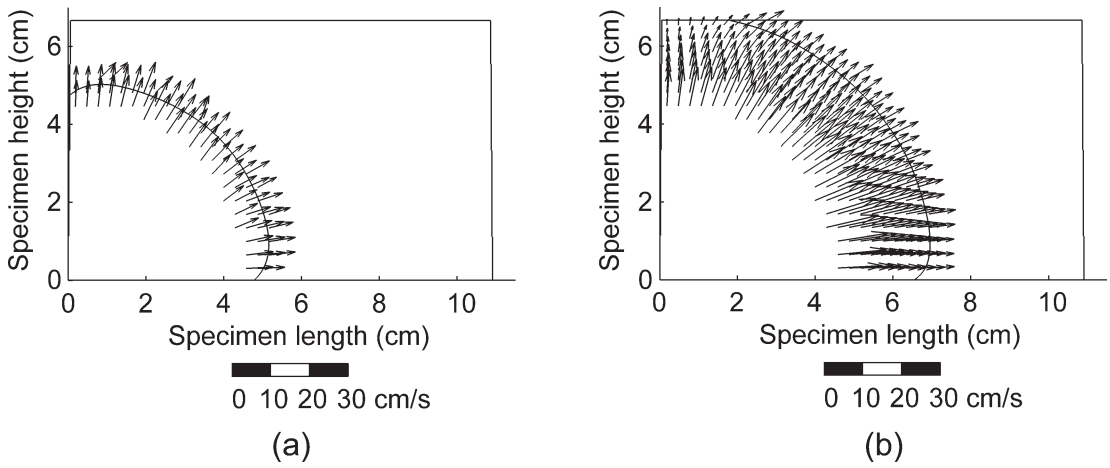


FIG. 1. Midplane velocity vectors for an injection flow rate of 34.5 $cm^3\ s^{-1}$, 245°C melt temperature, at (a) 30% and (b) 50% of the fill time.

 DOI 10.1002/pen

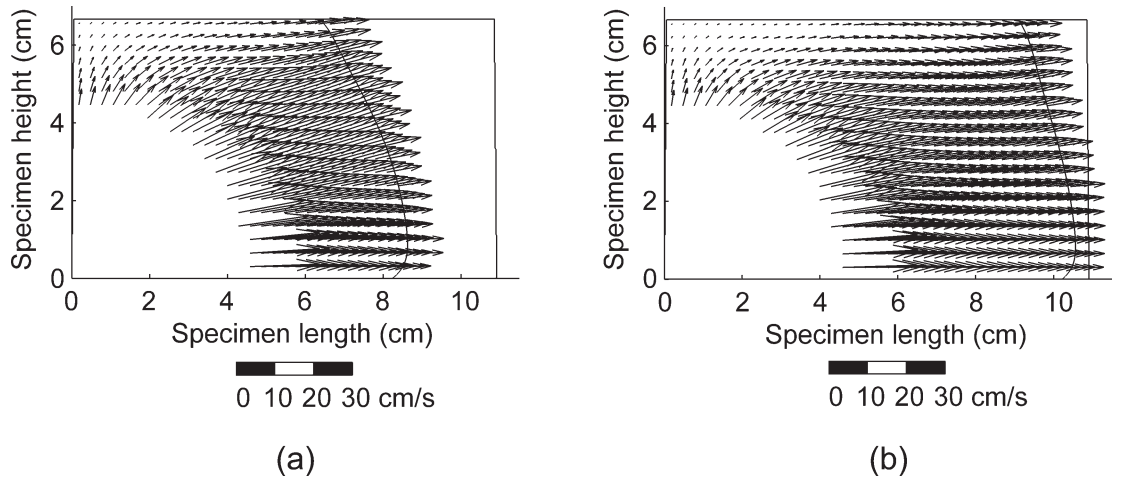


FIG. 2. Midplane velocity vectors for an injection flow rate of 34.5 $cm^3$ $s^{-1}$, 245°C melt temperature, at (a) 70% and (b) 90% of the fill time.

to the maximum velocity $u_{max}$ found at the center of the cavity:

$$u_{mean} = F u_{max} \tag{5}$$

Here the proportionality constant is the profile factor $F$. This assumption of proportionality holds true for flows with a self-similar velocity profile. A self-similar velocity profile is a normalized velocity profile that maintains its shape at all points in a flow field. The normalization factor is commonly the maximum velocity at a given streamwise position:

$$\frac{u}{u_{max}} = f(y/B) \tag{6}$$

where $y$ is a coordinate measuring distance perpendicular to the midplane of the cavity of width $2B$ and $f$ is a profile function. The maximum velocity $u_{max}$ can be a function of distance from the gate, temperature, injection rate, and other parameters. The profile function $f$ can only be a function of $y/B$. Self-similar velocity profiles for a Newtonian fluid and a power law fluid in a channel of width $2B$ are shown in Fig. 3.

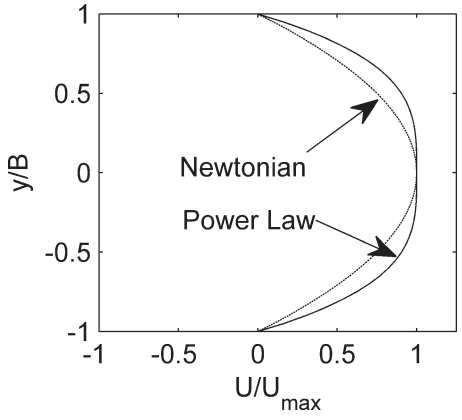


FIG. 3. Self-similar velocity profiles for Poiseuille flow of a Newtonian fluid and a power law fluid with $n = 0.4$.

The average velocity magnitude the self-similar profile described by *Eq. 6* can be calculated as:

$$u_{mean} = \frac{u_{max}}{2} \int_{-1}^{1} f(y/B) d(y/B) \tag{7}$$

From *Eqs. 5* and *7* it follows that the profile factor is:

$$F = \frac{1}{2} \int_{-1}^{1} f(y/B) d(y/B) \tag{8}$$

The injection rate can be used to estimate $F$ from the PIV data using a simple control volume analysis. A control surface $S$ for the mold cavity used in the present work is shown in Fig. 4. The vectors shown represent the PIV vectors $u_{max}$ at the midplane of the mold cavity along the right edge of the control surface. The coordinate $y/B$ is perpendicular to the page. $Q$ is the injection volume flow rate. In the experimental work of Bress and Dowling [15] $Q$ was calculated by dividing the cavity volume by the fill time. The fill time was measured directly from the digital movies of the mold filling process.

Applying the mass conservation equation, the volume flux through $S$ is calculated as follows:

$$Q = \int_S 2BF(u_{perp} \pm e_u) dS \tag{9}$$

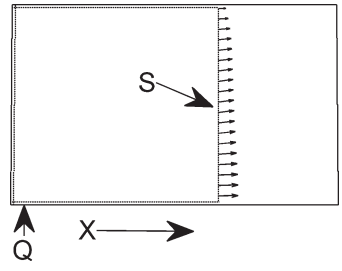


FIG. 4. Illustration of the control surface $S$ used for the volume flux and profile factor calculations in *Eqs. 9* and *10*.

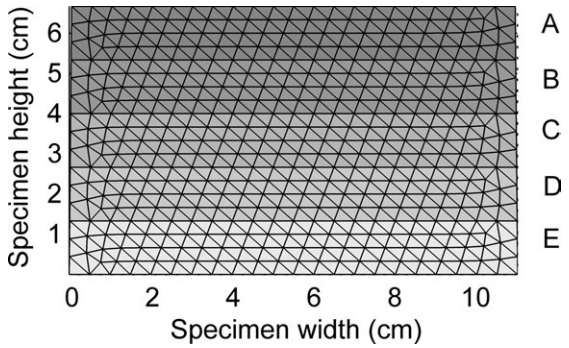


FIG. 5. Mesh used in the Moldflow simulation of the mold filling process. The shaded regions denote elements with constant assigned thickness. The thickness varies to account for draft in the mold cavity. The assigned element thicknesses are found in Table 2.

where $u_{perp}$ is the component of the PIV velocity perpendicular to the control surface, $e_u$ is the PIV velocity error, and $F$ is the profile factor. The cavity half-thickness $B$ has been left inside the integral to allow for the fact that $B$ varies slightly as a function of position within the cavity due to a slight draft within the mold that was necessary to aid molded-part extraction.

*Equation 9* can now be used to estimate the profile factor $F$. If it is assumed that $F$ is constant

$$F = \frac{Q}{\int_S 2B(u \pm e_u)dS} \tag{10}$$

*Equation 10* was used to estimate $F$ for all the molding conditions used in the study described in [15]. The PIV data at 90% of fill was examined for each PIV data set. For each PIV data set a series of control surfaces was used. Each surface resembled the one shown in Fig. 4. Taking the longest dimension of the cavity as the $x$ axis with the corner of the cavity as the origin, a series of control surfaces was constructed by selecting different $x$ coordinates for the portion of the surface that did not coincide with a cavity wall. The $x$ coordinate of this portion of the surface was always larger than the radius of the dead zone around the gate and smaller than the flow front location to avoid the fountain flow near the front. The value of $F$ was calculated for each control surface of each data set. The mean of the calculated values was $0.7 \pm 0.1$, where the error of 0.1 was twice the standard deviation of the set of calculated values of $F$.

The self-similar velocity profile of the Poiseuille flow of power law fluid with exponent $n$ in a channel of width $2B$ shown in Fig. 3 is given by [20]:

$$\frac{u}{u_{max}} = 1 - \left|\frac{y}{B}\right|^{\frac{n+1}{n}} \tag{11}$$

Substituting *Eq. 11* into *Eq. 10* gives $F = (n+1)/(2n+1)$. In Table 1 the shear-thinning exponent $n$ of the polymer-particle mixture is 0.342 yielding a power law profile factor $F = 0.79$, which falls within the calculated range $0.7 \pm 0.1$. The discrepancy between the power-law-exponent profile factor ($F = 0.79$) and the measured profile factor ($F = 0.7 \pm 0.1$) is most likely due to the actual flow profile not being fully self-similar.

### *Simulating the Mold Filling Flow With Moldflow*

Moldflow Plastics Insight version 6.1 was used to simulate the experimentally measured flow. A midplane mesh model of the cavity of the optical access mold used in [15] was constructed and is shown in Fig. 5. Summary statistics of the mesh can be found in Table 2. A midplane mesh is two-dimensional, but the assigned thickness of the elements can vary to reflect changes in the cavity thickness. In the optical access mold, draft on the large steel surface opposite the main window causes the cavity thickness to vary within the cavity. This was reflected in the midplane mesh and is illustrated in Fig. 5. The assigned element thicknesses are listed in Table 2.

Simulations were run for the same set of molding conditions used in the PIV experiments. The Moldflow results were then exported for further analysis. The element velocities were interpolated onto the same grid used by the PIV results. To facilitate comparison between the experimental data and simulation results the vector-free zone near the gate was mimicked in the simulation results.

The results of this processing are shown in Figs. 6 and 7. In these figures the interpolated Moldflow average velocity fields have been superposed by the cavity outline and the appropriate fill time contour to represent the flow front.

### *Comparison of the Simulated Flow Fronts With the Experimental Data*

Figure 8 shows a comparison between the experimentally measured flow fronts and the Moldflow simulation

TABLE 2. Statistics for the Moldflow mesh used to simulate the mold filling phase.

| | |
|---|---|
| **Entity counts** | |
| Surface triangles | 880 |
| Nodes | 478 |
| Mesh volume | 48.9511 $cm^3$ |
| Mesh area | 73.7051 $cm^2$ |
| **Surface triangle aspect ratio** | |
| Minimum aspect ratio | 1.233 |
| Maximum aspect ratio | 2.033 |
| Average aspect ratio | 1.535 |
| **Assigned element thicknesses** | |
| Region A | 6.408 mm |
| Region B | 6.641 mm |
| Region C | 6.525 mm |
| Region D | 6.757 mm |
| Region E | 6.874 mm |


DOI 10.1002/pen

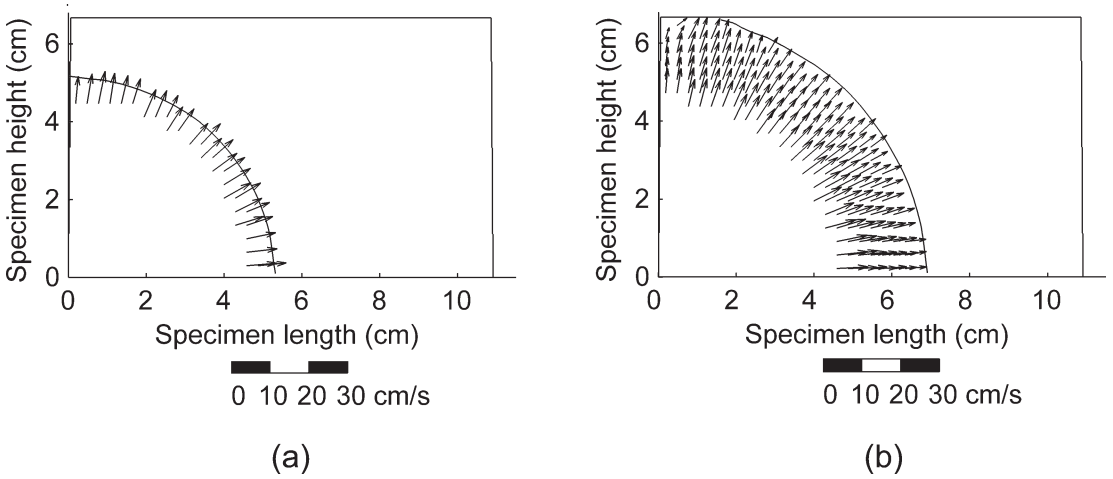


FIG. 6. Moldflow-generated average velocity vectors for an injection flow rate of 34.5 $cm^3\ s^{-1}$ of STYRON 615APR, 245°C melt temperature, at (a) 30% and (b) 50% of the fill time.

fronts at $t^* = 0.1$, 0.3, 0.5, 0.7, and 0.9 for specimens molded at 245°C and 34.5 $cm^3\ s^{-1}$. The striking feature of this figure is the difference between the data and the simulation near the cavity walls. This is due to the Hele–Shaw approximation, as described above. The simulated flow fronts will tend to be perpendicular to the walls when using the Hele–Shaw approximation. This is not what actually happens in the mold cavity. In the flow fronts extracted from the digital movies the fronts always curve toward the wall. Along a long straight wall the region of mismatch is expected to extend approximately one local cavity thickness from the wall [21]. Along the lower edge of Fig. 8, this dimension is $\sim$ 0.7 cm and matches the extent of the region of excess melt-front curvature.

The mismatch between the simulation and the extracted flow fronts along the walls and in the corners of the mold are inherent to the Hele–Shaw model, they are not experimental artifacts. Optical molds designed for observing melt flow must be carefully vented to avoid flow distortions due to trapped air in the mold. Air traps were not an issue in the mold used in [15]. The interface between the glass window and the steel cavity was not as air-tight as the steel–steel interfaces usually found in an injection mold, providing the air in the mold with a ready escape path without allowing flash.

Another feature of Fig. 8 is that the actual fronts lead the simulated fronts away from the cavity walls. This is due to the fountain flow effect. The actual fronts have curvature through the thickness of the cavity. Examination of a short shot would show that the flow front has a somewhat parabolic shape when viewed from the side. The manually extracted flow fronts trace out the tip of this profile. The simulation calculates an average velocity, which is constant through the thickness of the part. This means that the experimentally determined fronts will lead the simulated fronts, even if the two fronts enclose equal polymer volumes.

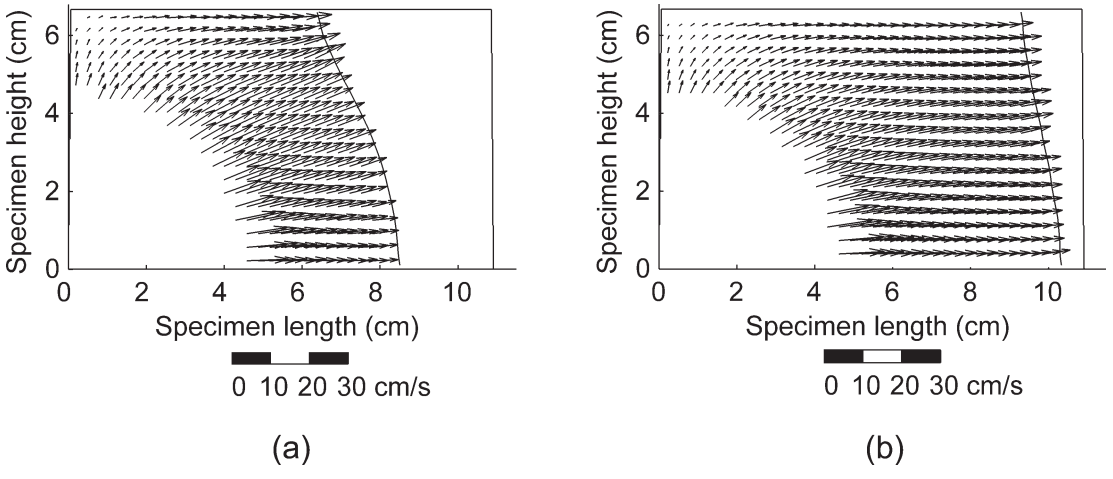


FIG. 7. Moldflow-generated average velocity vectors for an injection flow rate of 34.5 $cm^3\ s^{-1}$ of STYRON 615APR, 245°C melt temperature, at (a) 70% and (b) 90% of the fill time.

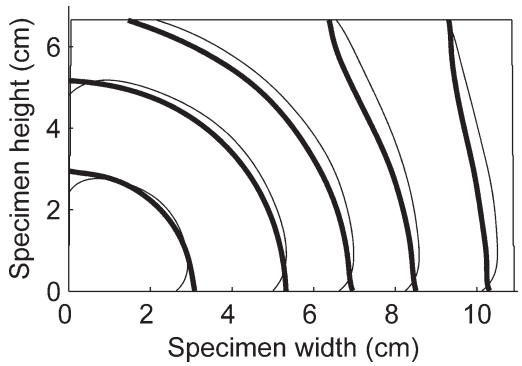


FIG. 8. Comparison of the simulation flow fronts (heavy lines) with those extracted manually from the digital movies of the mold filling (thin lines).

To quantify the differences between the measured and simulated flow fronts it is useful to recognize that at $t^* = 0.1$ and $t^* = 0.3$ the flow fronts are primarily radial. A polar coordinate system was defined for these two data sets as shown in Fig. 9a. The normalized residuals of the $r$ components of the points on the fronts were calculated for values of $\theta$ ranging from 0° to 90° and are plotted in Fig. 9b. The simulated fronts were most accurate in the middle of the cavity and had high residuals near the walls.

The flow fronts transition from radial to primarily channel flow between $t^* = 0.3$ and $t^* = 0.5$. The fronts at $t^* = 0.5$, $t^* = 0.7$, and $t^* = 0.9$ are more conveniently analyzed using a Cartesian coordinate system as shown in Fig. 10a. The coordinates of the points on the fronts were transformed to the reference frame illustrated in Fig. 10a and the normalized residuals of the $x$ coordinates were calculated for values ranging over the specimen height from 0 to 6.7 cm. The results are plotted in Fig. 10b. Again, the simulated fronts are most accurate near the middle of the cavity but have significant residuals near the walls.

*Comparison of the Simulated Velocity Fields With the Experimental PIV Data*

Both the PIV and simulated vector fields are confined to the midplane of the mold, so both fields have two components and thus two comparisons need to be made. Rather than examine the Cartesian velocity components it is more convenient to compare velocity magnitudes and orientations. This is due to the limitations of both the PIV experimental method and the Hele–Shaw model. The Hele–Shaw method predicts average velocity vectors whose orientation is constant throughout the thickness of the part. The PIV experimental method does not produce average velocities directly, but the orientation of the measured velocities at a given point and given instant of time are also likely to be constant throughout the thickness of the part. This suggests that decoupling the orientation and magnitude comparisons would be fruitful.

To compare velocity vector orientations the vector angles were calculated at each point in the $t^* = 0.9$ field and in the corresponding PIV vector field. A scalar field was created by subtracting the simulated velocity orientations from the PIV velocity orientations at each point in the field. A contour plot of this orientation differences is shown in Fig. 11. The contour plot is presented with the simulation results for ease of reference.

A set of all of the orientation differences in the field was then created and summary statistics for this set were calculated. Figure 12 shows a histogram of the velocity orientation differences shown in Fig. 11. This figure shows that the predicted orientations are quite good, with a mean angular difference of only 0.9°. The standard deviation of the orientations was 3.2°. The histogram shows some outliers at the low end of the range. These outliers correspond to the velocities measured near the corner of the mold opposite the gate, as seen in Fig. 11. The region near the upper portion of the front is also a region of relatively high orientation error, although not as severe as the corner of the mold.

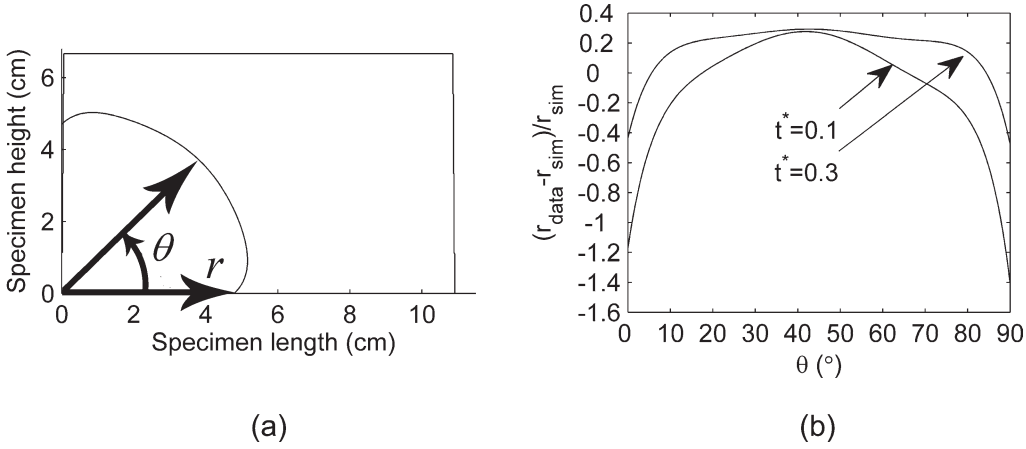


FIG. 9. (a) Polar coordinate system used to compare the measured and simulated flow fronts at $t^* = 0.1$ and $t^* = 0.3$ (b) Comparison of extracted and simulated fronts at $t^* = 0.1$ and $t^* = 0.3$.

 DOI 10.1002/pen

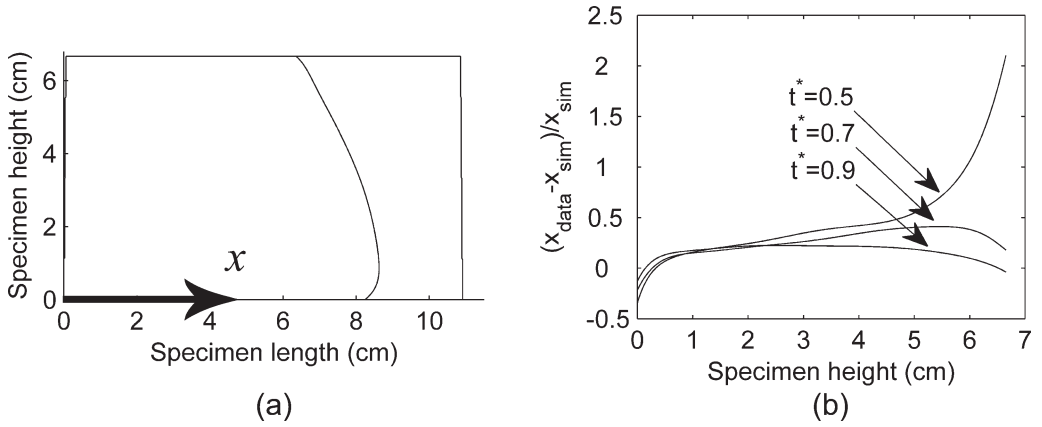


FIG. 10. (a) Cartesian frame of reference used for comparing the measured and simulated fronts at $t^* = 0.5$, $t^* = 0.7$, and $t^* = 0.9$ (b) Comparison of extracted and simulated fronts at $t^* = 0.5$, $t^* = 0.7$, and $t^* = 0.9$.

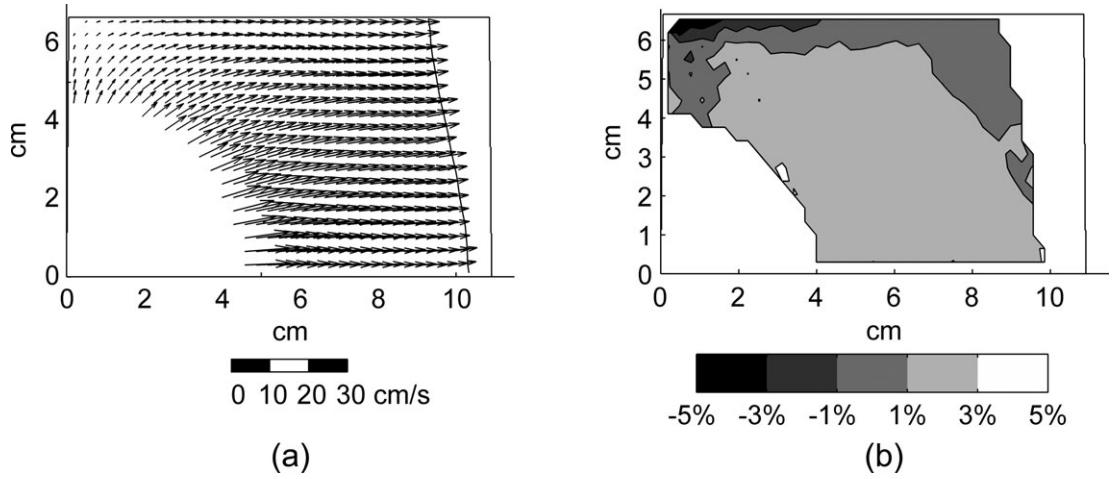


FIG. 11. Side by side comparison of (a) the simulation results for $t^* = 0.9$ and (b) a contour plot of the difference in degrees of the experimentally measured velocity orientations and the simulated velocity orientations.

To compare the measured and simulated velocity magnitudes the thickness-averaged velocity magnitudes of the PIV data must be calculated by assuming a profile factor. In the channel-flow region of the mold filling process the average profile factor $F$ was 0.7. If this factor is applied to the entire field an estimated average velocity field can be calculated as $u_{mean} = Fu_{max}$. The estimated average velocity field can then be compared to the simulation results, as shown in Fig. 13. The contour plot in Fig. 13 represents the ratio of the magnitude of the PIV vectors to the magnitude of the simulated vectors and is presented with the simulation results for reference.

The magnitude ratios were then collected into a set and summary statistics were calculated. Figure 14 shows a histogram of the velocity magnitude ratios plotted in Fig. 13. In general the comparison is quite good, with the mean ratio of magnitudes equal to 0.99 and a standard deviation of 0.25. Figure 14 contains outliers at the lower end of the range. These outliers correspond to velocity vectors found in the corner opposite the gate, as seen in Fig. 13. The region behind the upper portion of the front also has a relatively high magnitude ratio error, though not as severe as in the corner.

These two areas, the corner and the front, are problematic for both the velocity orientation and magnitude

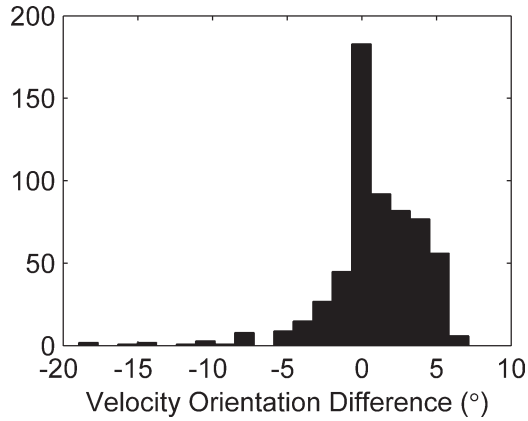


FIG. 12. Histogram of the velocity orientation differences plotted in Fig. 11(b). The mean angular difference is 0.9° and the standard deviation is 3.2°.

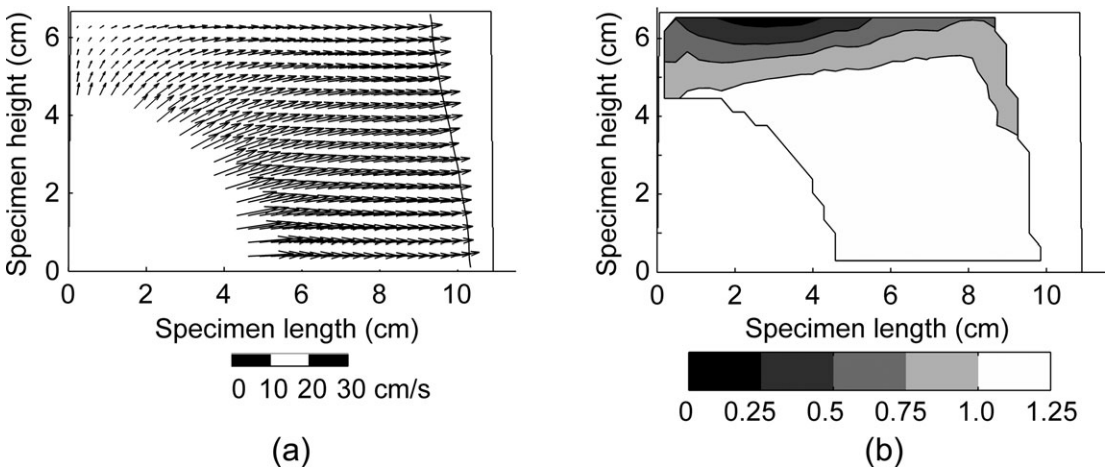


FIG. 13. Side by side comparison of (a) the simulation results for $t^* = 0.9$ and (b) a contour plot of the ratio of the estimated average PIV velocity magnitude to the simulated average velocity magnitude.

predictions. This is likely due to a combination of two factors.Near the walls the simulation is likely to have a higher velocity since the Hele–Shaw approximation does not impose the no-slip boundary condition. Second, near the corner the flow is transitioning from radial to channel flow. This means that the profile factor calculated from the purely channel-flow regime is probably not as applicable in this region. Also the measured velocities in the corner region are much smaller than those in the rest of the field and so the PIV data has the lowest signal-to-noise ratio in this region of the flow.

## CONCLUSIONS

This article presents comparisons between experimental midplane velocity vector fields measured in a polystyrene melt as it fills an injection mold and a Moldflow simulation of the same flow. The following conclusions can be drawn from this study. (1) Discrepancies between the experimentally measured and simulated flow fronts were noted and quantified, particularly at the cavity walls. These discrepancies are consistent with known limitations of the Hele–Shaw approximation used by Moldflow. (2) Comparison of the simulated flow fronts with fronts extracted from the digital movies show that the simulated fronts are least accurate near the cavity walls. (3) To make a comparison between experimentally measured midplane velocity vectors and the average velocity vectors reported by Moldflow, a profile factor needed to be calculated. This can be done using a control volume analysis and the known injection rate. In this study the average profile factor was found to be $0.7 \pm 0.1$ which is generally consistent with measured rheological properties of the molten plastic used in this study. (4) Quantitative comparisons of the simulation results and the PIV data showed that the simulation agreed well with the data. The mean value of the ratio of the magnitude of the PIV vectors to that of the simulation was 0.99 with a standard deviation of 0.25. The mean value of the difference between the orientations of the PIV data and the simulation was $0.9^\circ$ with a standard deviation of $3.2^\circ$. The corner area opposite the gate was most problematic for both the simulated velocity magnitudes and orientations. The velocities near the front also had relatively high simulation errors, though not as severe as those in the corner.

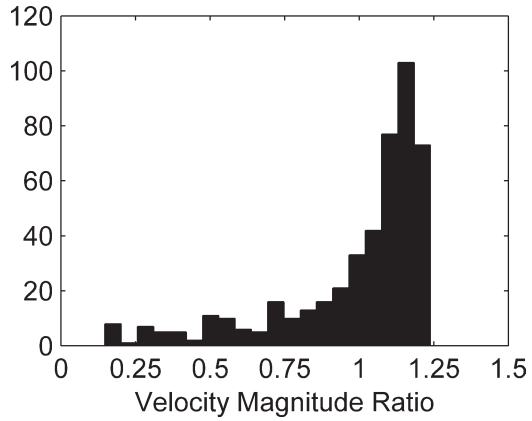


FIG. 14. Histogram of the velocity magnitude ratio plotted in Fig. 13(b). The mean magnitude ratio is 0.99 and the standard deviation is 0.25.

## ACKNOWLEDGMENTS

Plastics Provisions and Cincinnati Milacron assisted with the purchase of the injection molding machine.

## REFERENCES

1. J. Dealy and K. Wissbrun, *Melt Rheology and its Role in Plastics Processing*, Van Nostrand Reinhold, New York (1990).
2. J. Shoemaker, *Moldflow Design Guide: A Resource for Plastic Engineers*, Hanser Gardner Publications, Cincinnati (2006).

3. D. Kazmer, R. Nageri, V. Kudchakar, B. Fan, and R. Gao, *Polym. Eng. Sci.*, **46**, 274 (2006).
4. G. Gilmore and S. Spencer, *Mod. Plast.*, **28**, 117 (1951).
5. M. Kamal and S. Kenig, *Polym. Eng. Sci.*, **12**, 302 (1972).
6. J. White and H. Dee, *Polym. Eng. Sci.*, **14**, 212 (1974).
7. M. Kamal and S. Kenig, *Polym. Eng. Sci.*, **12**, 294 (1972).
8. J. White, *Polym. Eng. Sci.*, **15**, 44 (1975).
9. S. Fathi and A.H. Behravesh, *Polym. Eng. Sci.*, **47**, 750 (2007).
10. S. Fathi and A.H. Behravesh, *Polym. Eng. Sci.*, **48**, 598 (2008).
11. L. Tredoux, I. Satoh, and Y. Kurosaki, *Polym. Eng. Sci.*, **40**, 2161 (2000).
12. X. Han and H. Yokoi, *Polym. Eng. Sci.*, **46**, 1590 (2006).
13. M. Raffel, C. Willert, and J. Kompenhans, *Particle Image Velocimetry: A Practical Guide*, Springer-Verlag, Berlin (1998).
14. B. Baumert, D. Liepmann, and S. Muller, *J. Non-Newt. Fluid Mech.*, **69**, 221 (1997).
15. T. Bress and D. Dowling, *Polym. Eng. Sci.*, **51**, 730 (2011).
16. T. Bress and D. Dowling, *J. Reinforc. Plast. Compos.*, **17**, 1374 (1998).
17. C. Willert and M. Gharib, *Exp. Fluids*, **10**, 181 (1991).
18. J. Dantzig and C. Tucker, *Modeling in Materials Processing*, Cambridge University Press, Cambridge (2001).
19. D. Coyle, J. Blake, and C. Macosko, *AIChE J.*, **33**, 1168 (1987).
20. C. Rauwedaal, *Polymer Extrusion*, 4th ed., Hanser Gardner Publications, Cincinnati (2001).
21. P.K. Kundu, I.M. Cohen, and D.R. Dowling, *Fluid Mechanics*, 5th ed., Academic Press, Waltham, MA, 357 (2012).